IRSTI 29.05.41; 29.05.45 https://doi.org/10.26577/ijmph.20211226

RELATIVISTIC INTERIOR SOLUTIONS FOR WHITE DWARFS: TESTING TOLMAN AND VAIDYA–TIKEKAR MODELS AGAINST QUANTUM STATISTICAL EQUATIONS OF STATE

V. Ollivier [1*], **M. S. Mansur** [2], **N. Beissen** [2] and **A. Abylayeva** [2]

[1] *École polytechnique, Palaiseau, France*

[2] *Al-Farabi Kazakh National University, Almaty, Kazakhstan*

Email: viren.olliver@polytechnique.org

(Received 1 July 2026; revised 24 October 2026; accepted 2 November 2026)

Abstract. White dwarfs are supported by degenerate electron pressure, yet it is unclear whether exact general relativistic interior solutions can describe them. We test the Tolman IV, Tolman VII, and Vaidya–Tikekar (VT) solutions against the Chandrasekhar and Salpeter equations of state (EOS) for central densities 10^4–$10^{12}\,\mathrm{g\,cm^{-3}}$, using the EOS curvature, mass–radius diagrams, and interior density and pressure profiles. The Tolman IV EOS is concave, whereas both quantum statistical EOS are strictly convex; with Chandrasekhar central values its maximum mass is only about $0.4\,M_\odot$, and at the observed radii of Sirius B and 40 Eridani B it gives 0.10 and $0.04\,M_\odot$ instead of 1.02 and $0.57\,M_\odot$. The Tolman VII density profile lies above both quantum statistical profiles at every interior radius for $0.7 \le \mu \le 1$ (RMSD 0.19–0.60). The limiting VT profile also lies above the Chandrasekhar one; a two-parameter extension reduces the RMSD to 0.04–0.07, but its density cannot vanish at a finite radius and its mass exceeds the Chandrasekhar value by 38–140%. None of the three solutions is therefore compatible with white dwarf microphysics; other exact solutions are not excluded.

Keywords: white dwarfs; general relativity; exact interior solutions; Tolman solutions; Vaidya–Tikekar; equation of state; mass–radius relation

1. INTRODUCTION

White dwarfs are the end products of stellar evolution for the vast majority of stars, including our Sun, and represent one of the most abundant classes of compact objects in the Galaxy. With masses typically below the Chandrasekhar limit of approximately $1.4\,M_\odot$ and radii comparable to that of the Earth, white dwarfs occupy a unique position in astrophysics: they are only weakly relativistic ($GM/Rc^2 \sim 10^{-4}$), so general relativistic corrections to the stellar structure equations are small, although they grow with central density, and their internal pressure is dominated not by nuclear or hadronic interactions but by the quantum mechanical degeneracy of electrons [1, 2, 3].

The theoretical foundation for white dwarf structure was laid by Chandrasekhar in the 1930s [4, 5], who derived the equation of state for a zero-temperature relativistic degenerate electron gas using Fermi–Dirac statistics. This framework yields a parametric equation of state in which both pressure and density are expressed as functions of the dimensionless Fermi momentum $y = p_F/(m_e c)$. A crucial consequence is the existence of a maximum mass — the Chandrasekhar limit — beyond which electron degeneracy pressure is insufficient to support the star against gravitational collapse [1]. Subsequent work by Salpeter [6] refined this picture by incorporating Coulomb lattice energy, Thomas–Fermi electron screening, exchange effects, and correlation corrections. These contributions, though subdominant at high densities, systematically reduce the pressure at fixed density and are particularly significant in the low-density regime relevant to He, C, O, and Fe white dwarfs [6, 7, 8, 9, 10, 11, 12, 13].

In parallel, the problem of finding exact interior solutions to Einstein's field equations for relativistic stars has attracted sustained attention since Schwarzschild's pioneering work on uniform-density stars [14]. Tolman [15]

 © 2026 Al-Farabi Kazakh National University

systematically classified a family of exact static, spherically symmetric solutions — now known as Tolman I through VIII — that provide analytical expressions for the metric functions, pressure, and density without specifying an equation of state apriori. Among these, Tolman IV and Tolman VII have proven particularly useful as interior solution ansätze for neutron stars and other compact objects, owing to their regularity at the center, physically reasonable density profiles, and algebraic tractability [15, 16, 17]. The Vaidya–Tikekar model [18] extends this program by adopting a spheroidal spatial geometry parametrised by a single geometric constant K, and has been widely applied to superdense relativistic stars, including neutron stars and quark stars [19, 20, 21, 22].

A natural question arises: can these successful geometric interior solutions, validated against neutron star observations [16, 23, 24, 25], also describe the interior structure of white dwarfs when paired with the Chandrasekhar or Salpeter equations of state? This question is physically motivated because white dwarfs and neutron stars share several structural features — spherical symmetry, hydrostatic equilibrium, and the relevance of general relativistic corrections at the highest densities — yet their microphysics differ fundamentally. For neutron stars, the equation of state at supranuclear densities is concave in the p–ρ plane, a feature naturally reproduced by geometric interior solutions [16, 23]. For white dwarfs, however, the electron degeneracy equation of state is strictly convex across the entire relevant density range $\rho_c = 10^4$–$10^{12}\ \mathrm{g\,cm^{-3}}$, raising the question of whether this microphysical constraint can be accommodated by any of these purely geometric models.

Several works have attempted to extend geometric interior solutions to white dwarfs or other compact objects across a wide density range. Bowers and Liang [26] and, more recently, various authors [27, 28] have constructed anisotropic or generalised interior solutions and applied them to compact objects. Beyond these geometric extensions, a substantial and more recent body of work addresses white dwarf structure through improved microphysics rather than modified geometry: finite-temperature corrections [29, 30], rotation [31, 32, 9, 33, 34], strong magnetic fields [35], and anisotropic pressure have each been shown to shift the mass–radius relation away from the classical Chandrasekhar prediction. In this context, simplified frameworks such as one-dimensional Newtonian reductions with rotation-induced effective anisotropy have also been developed to analyze uniform rotation trends [36]. Complementary studies have also examined inverse stellar-structure problems, reconstructing an equation of state directly from an assumed metric [37]. The present work is orthogonal to these efforts: rather than modifying the microphysics or geometry to improve agreement, we test whether *unmodified*, literature-standard geometric ansätze are, on their own, compatible with the unmodified, literature-standard white dwarf equation of state. However, a systematic comparison of the curvature properties of these field equation models against quantum statistical equations of state, focusing specifically on the white dwarf regime, has not, to our knowledge, been carried out.

While the individual analytical machinery employed here – curvature arguments, mass–radius integration, and monotonicity bounds – is standard, its systematic application to white dwarfs has, to our knowledge, not been previously reported. Tolman IV, Tolman VII, and Vaidya–Tikekar are workhorse solutions for neutron and quark stars, where the concave, supranuclear equation of state is compatible with their curvature properties by construction; whether the same compatibility extends to the qualitatively different, strictly convex electron-degeneracy regime of white dwarfs has not been established a priori. Our contribution is therefore to make this incompatibility explicit and quantitative, and to identify *why* it occurs, providing a concrete criterion that can be applied to test the applicability of any future geometric ansatz to white dwarf matter, rather than relying on a case-by-case numerical check.

In this paper, we perform precisely this comparison. Our approach proceeds along three complementary lines of evidence. First, we analyse the curvature of the equation of state for each field model and for the quantum statistical equations of state, establishing an analytic incompatibility criterion based on the sign of $d^2p/d\rho^2$. Second, we compute mass–radius diagrams for Tolman IV and normalised density profiles for Tolman VII, initialised with central conditions derived from the Chandrasekhar equation of state, and compare them directly with quantum statistical predictions. Third, for the Vaidya–Tikekar model, where the pressure is not easily extracted analytically, we focus on density profiles $\rho(r)$ at fixed central densities and exploit the monotonicity in K to derive a bounding argument. We further introduce a modified Vaidya–Tikekar model with a free parameter K_2 and assess whether this additional degree of freedom is sufficient to achieve compatibility.

The paper is organised as follows. The exterior Schwarzschild solution and the matching conditions at the stellar surface are collected in Appendix 5. The Methods section outlines our overall approach and introduces the Chandrasekhar and Salpeter equations of state and their numerical solutions for He, C, O, and Fe white dwarfs [6, 7, 8, 38]. The Field Equations section presents the three field equation models — Tolman IV, Tolman VII, and Vaidya–Tikekar — and derives their key analytical properties. Results and Discussion carries out the three-pronged comparison and establishes the incompatibility results. We conclude with a discussion of the physical implications and directions for future work.

2. METHODS

We test the compatibility of three exact general relativistic interior solutions with white dwarf matter by following a uniform procedure for each model. First, we review the Chandrasekhar and Salpeter quantum statistical equations of state, which provide the reference equation of state, mass–radius diagram, and density/pressure profiles against which the geometric models are tested. Second, for each field equation model — Tolman IV, Tolman VII, and the Vaidya–Tikekar model — we revisit the derivation of the interior density and pressure analytically from Einstein's field equations, expressed in terms of the central density ρ_c (and, where needed, the central pressure p_c) so that the models can be initialised on the same footing as the quantum statistical equations of state. Third, we apply a comparison criterion suited to each model: for Tolman IV, the sign of $d^2p/d\rho^2$ is used to test the curvature compatibility of its equation of state with the strictly convex quantum statistical equations of state, and this is cross-checked numerically via the mass–radius diagram;

for Tolman VII, whose density profile is a parabola controlled by a self-boundedness parameter $\mu \in [0,1]$ [39], we compare the normalised density profile, for a representative range of μ, directly against the Chandrasekhar and Salpeter profiles at several central densities. we also compare $\rho(r)$ for a range of μ and $p(\rho)$ with the Chandrasekhar and Salpeter ones (Appendix 5);

for the Vaidya–Tikekar model, where the pressure is closed-form only in the Newtonian limit, we compare density profiles at fixed central density and exploit the monotonicity of ρ in the geometric parameter K to derive a bounding argument relative to the Chandrasekhar prediction, and we further introduce a modified two-parameter extension (with free parameter K_2) to test whether the additional freedom restores compatibility.

a. Chandrasekhar's model

For white dwarfs, the most common way to obtain an expression for pressure and density is to use quantum statistics.

Thermodynamics of the degenerate electron gas

Consider electrons in a volume V with Fermi–Dirac occupation $f(p) = [\exp((E_p-\mu)/k_BT)+1]^{-1}$, $E_p = \sqrt{p^2c^2+m_e^2c^4}$. For $T \to 0$, $f(p) = \Theta(p_F - p)$ and the number density, energy density and

pressure are

$$
\begin{aligned}
n_e &= \frac{p_F^3}{3\pi^2\hbar^3}, \\
\varepsilon_e &= \frac{1}{\pi^2\hbar^3}\int_0^{p_F} E_p\, p^2\, dp, \\
P_e &= \frac{1}{3\pi^2\hbar^3}\int_0^{p_F} \frac{p^2c^2}{E_p}\, p^2\, dp,
\end{aligned}
\tag{1}
$$

where P_e gives Eq. (4). They satisfy $P_e = -\partial E/\partial V|_N$ and $\varepsilon_e + P_e = \mu\, n_e$. The ions only ensure charge neutrality and carry the mass density $\rho = (A/Z)\, m_n\, n_e$. Recent work has also formulated thermodynamic acceptability conditions for exact perfect-fluid solutions, including Tolman IV [40]; here we instead test their compatibility with the degenerate electron gas equation of state.

Assumptions

1. Electrons as a completely degenerate Fermi gas at $T = 0$ K,
2. Non-interacting electron gas,
3. Relativistic treatment of electrons,
4. Uniform composition,
5. Ions provide density but not pressure, and electrons provide pressure but not density,
6. No nuclear reactions or evolution.

The assumption of a completely degenerate gas at $T = 0$ K is justified by comparing the relativistic Fermi temperature T_F to the typical interior temperature of a white dwarf. Defining T_F via the relativistic Fermi kinetic energy,

$$
k_B T_F = m_e c^2 \left(\sqrt{1+y^2} - 1\right), \tag{2}
$$

with $y = p_F/(m_e c)$ as before, one finds that T_F ranges from approximately 10^8 K at a lower density of $\rho_c = 10^4$ g cm^{-3} to about 5×10^{11} K at a high-density regime of $\rho_c = 10^{12}$ g cm^{-3} relevant to white dwarfs, whereas typical interior temperatures are of order $T \sim 10^6$–10^7 K [2, 3]. While the condition $T \ll T_F$ holds strictly throughout the high-density core of the star, at the lowest density regime, the ratio becomes $T/T_F \approx 0.1$ (assuming $T \sim 10^7$ K). Since thermal excitations populate only a small fraction of states near the Fermi surface, the finite-temperature correction introduces a relative error of order $(T/T_F)^2 \sim 1\%$ [2]. This justifies neglecting finite-temperature corrections throughout the bulk of the configuration, while naturally accommodating the slight observational discrepancies in the outer layers of specific white dwarfs like Sirius B, which are widely attributed to thermal effects.

Equations

We have:

$$
\rho(r) = \frac{m_n}{3\pi^2}\left(\frac{m_e c}{\hbar}\right)^3 \left(\frac{A}{Z}\right) y^3(r) \tag{3}
$$

$$
\begin{aligned}
p(r) = \frac{m_e c^2}{24\pi^2}\left(\frac{m_e c}{\hbar}\right)^3 \\
\times \Big[y(r)\left(2y^2(r) - 3\right)\sqrt{1+y^2(r)} \\
+ 3\ln\left(y(r) + \sqrt{1+y^2(r)}\right)\Big]
\end{aligned}
\tag{4}
$$

where c is the speed of light in vacuum, $\hbar$ is the reduced Planck constant, $y(r) = p_F(r)/(m_e c)$, $m_{n,e}$ are the masses of a neutron and an electron respectively, p_F is the Fermi momentum of the electron, and A/Z is the average atomic mass number per electron.

We use two additional equations that relate the radial coordinate to the Fermi momentum. Using the Tolman–Oppenheimer–Volkoff (TOV) equation [41, 15] with G the gravitational constant, $m(r)$ the mass profile, with the total stellar mass given by $M \equiv m(R)$:

$$
\frac{dm(r)}{dr} = 4\pi r^2 \rho(r) \tag{5}
$$

$$\frac{dp(r)}{dr} = -\frac{G\rho(r)m(r)}{r^2}\left(1+\frac{p(r)}{\rho(r)c^2}\right) \times \left(1+\frac{4\pi r^3 p(r)}{m(r)c^2}\right) \times \left(1-\frac{2Gm(r)}{rc^2}\right)^{-1} \quad (6)$$

b. Salpeter's model

Chandrasekhar's approach models white dwarfs as an ideal relativistic degenerate electron gas, where both the pressure and the energy density arise from quantum statistics and are functions of the electron Fermi momentum.

Salpeter's approach extends this framework by including interaction corrections, namely Coulomb lattice energy, Thomas–Fermi corrections, electron exchange effects, and correlation energy. This leads to a modified pressure and a more realistic equation of state, especially at lower densities.

New assumptions

Salpeter makes the following different assumptions:

1. **Electron-electron Coulomb exchange interactions** are included, accounting for the electrostatic exchange energy between degenerate electrons (a correction beyond the pure Fermi-Dirac statistics of the ideal gas),

2. **Ions are treated as point charges arranged in a periodic lattice**, contributing an electrostatic lattice (Coulomb) energy — via a Wigner-Seitz cell treatment — rather than merely serving as a uniform, non-interacting background that ensures charge neutrality,

3. **The electron density is allowed to be non-uniform**, exhibiting a slight polarization (accumulation) around each ion within its Wigner-Seitz cell, instead of being treated as a perfectly uniform background as in the Chandrasekhar model.

Corrected equation of state

The Coulomb and Thomas–Fermi effects give:

$$p_c + p_{TF} = -mc^2\left(\frac{mc}{\hbar}\right)^3\left[\frac{\alpha Z^{2/3}}{10\pi^2}\left(\frac{4}{9\pi}\right)^{1/3}y^4 + \frac{162}{175}\frac{(\alpha Z^{2/3})^2}{9\pi^2}\left(\frac{4}{9\pi}\right)^{2/3} \times \frac{y^5}{\sqrt{1+y^2}}\right] \quad (7)$$

Zapolski's exchange term gives, using $\beta = y + \sqrt{1+y^2}$:

$$p_{ex} = -\frac{\alpha}{4\pi^3}mc^2\left(\frac{mc}{\hbar}\right)^3\left\{\frac{1}{32}\left(\beta^4+\beta^{-4}\right)+\frac{1}{4}\left(\beta^2+\beta^{-2}\right) -\frac{9}{16}-\frac{3}{4}\left(\beta^2-\beta^{-2}\right)\ln\beta+\frac{3}{2}(\ln\beta)^2 -\frac{y}{3}\left[1+\frac{y}{\sqrt{1+y^2}}\right] \times\left[\frac{1}{8}\left(\beta^3-\beta^{-5}\right)-\frac{1}{4}\left(\beta-\beta^{-3}\right) -\frac{3}{2}\left(\beta+\beta^{-3}\right)\ln\beta+\frac{3}{\beta}\ln\beta\right]\right\} \quad (8)$$

The correlation term:

$$p_{cor} = -\frac{0.0311}{9\pi^2}m_e c^2\left(\frac{m_e c}{\hbar}\right)^3\alpha^2 y^4 \quad (9)$$

where Z is the atomic number and $\alpha \approx 1/137$ is the fine-structure constant. The total Salpeter pressure is then:

$$p_{\text{Salpeter}} = p_{\text{Chandrasekhar}} + p_c + p_{TF} + p_{ex} + p_{cor} < p_{\text{Chandrasekhar}} \quad (10)$$

c. Numerical procedure

To obtain the mass–radius relation for each composition, we solved the TOV equations, Eq. (5)–(6), numerically in Python using the

Chandrasekhar and Salpeter equations of state as input. Each integration was initialised at a range of central densities 10^4–10^{12} g·cm^{-3} and carried out for $Z = 2, 6, 8, 26$, corresponding to helium, carbon, oxygen, and iron white dwarfs respectively, with the integration terminated at the stellar surface where $p(r) \to 0$.

3. Field Equations

a. Tolman IV

The Tolman IV solution is an exact static, spherically symmetric solution of Einstein's field equations. It is commonly used as an analytical ansatz to describe the interior spacetime of relativistic stars. It provides regular metric functions and finite central density and pressure, making it suitable for constructing physically acceptable stellar models. It is typically applied to compact objects such as neutron stars and other dense stellar remnants.Before specifying the interior, we recall the exterior region. Outside a static, spherically symmetric, uncharged star the vacuum solution is the Schwarzschild metric, and any interior solution must be joined to it at $r = R$ (see Appendix 5 for the exterior solution, the Tolman IV interior written in terms of M and R, and the matching).

Assumptions

Tolman IV is based on General Relativity and makes the following assumptions:

1. Thanks to the spherical symmetry of the system, the metric can be written in the form:
$$ds^2 = e^{\nu}\,dt^2 - e^{\lambda}\,dr^2 - r^2(d\theta^2 + \sin^2\theta\,d\varphi^2) \tag{11}$$
where ν and λ are functions of r only.

2. The stellar matter is a perfect fluid, so that:
$$T^{\mu\nu} = \left(\rho + \frac{p}{c^2}\right) u^{\mu}u^{\nu} + p\,g^{\mu\nu} \tag{12}$$
where p is the pressure and ρ is the density.

3. At the surface of the star, the metric must match the exterior Schwarzschild solution (Appendix 5):
$$e^{\nu(R)} = 1 - \frac{2GM}{c^2R} \tag{13}$$
$$e^{\lambda(R)} = \left(1 - \frac{2GM}{c^2R}\right)^{-1} \tag{14}$$
where R is the stellar radius and $m(R) = M$.

4. The following condition is assumed:
$$\frac{e^{\nu}\nu'}{2r} = \text{constant}. \tag{15}$$

Consequences

By using spherical symmetry and energy-momentum tensor, we recall this following result :

$$\frac{8\pi G\rho(r)}{c^2} = \frac{1}{r^2}\frac{d}{dr}\left(r\left(1 - e^{-\lambda(r)}\right)\right) \tag{16}$$

We denote the stellar radius by R throughout, and use A and D for the free constants of the metric ansatz. Denoting A and D as free constants, the field equations yield: Defining $a \equiv A^2/D^2$ and $u \equiv 1 + 2r^2/A^2$, the density and pressure take the compact form

$$\frac{8\pi G}{c^2}\rho = \frac{1}{A^2}\left[\frac{2+a}{u^2} + \frac{1+a/2}{u} + \frac{3a}{2}\right] \tag{17}$$

$$\frac{8\pi G}{c^4}p = \frac{1}{A^2}\left[\frac{1+a/2}{u} - \frac{3a}{2}\right] \tag{18}$$

Useful parameters

The stellar radius R is obtained from the physical condition $p(R) = 0$. Tolman finds:

$$R = \frac{D}{\sqrt{3}}\left(1 - \frac{A^2}{D^2}\right)^{1/2} \tag{19}$$

Moreover, continuity of the metric at the stellar surface requires the interior Tolman solution to match the exterior Schwarzschild metric (Appendix 5). This yields:

$$\frac{MG}{c^2} = \frac{R}{2}\left\{1 - \frac{(1 - R^2/D^2)(1 + R^2/A^2)}{1 + 2R^2/A^2}\right\} = \frac{R^3}{A^2}\frac{1 - R^2/D^2}{1 + 2R^2/A^2} = \frac{R^3}{D^2} \tag{20}$$

where M is the total mass of the star.

Given the total mass and radius of the star, the constants A and D are fully determined. Note that $D > A$ follows from Eq. (19).

Denoting by ρ_c and p_c the central density and pressure respectively, we have:

$$\frac{8\pi G}{c^2}\rho_c = \frac{3\,(A^2+D^2)}{A^2D^2} \tag{21}$$

$$\frac{8\pi G}{c^4}p_c = \frac{D^2-A^2}{A^2D^2} \tag{22}$$

Inverting these relations gives:

$$A^2 = \frac{3c^4}{4\pi G(c^2\rho_c+3p_c)} \tag{23}$$

$$D^2 = \frac{3c^4}{4\pi G(c^2\rho_c-3p_c)} \tag{24}$$

which requires $c^2\rho_c > 3p_c$.

Substituting into Eq. (19):

$$R^2 = \frac{D^2-A^2}{3} = \frac{3c^4\,p_c}{2\pi G\,(c^4\rho_c^2-9p_c^2)} \tag{25}$$

From these considerations, Tolman derives a relation between ρ and p:

$$\rho c^2 = c^2\rho_c - 5(p_c-p) + 8\,\frac{(p_c-p)^2}{c^2\rho_c+p_c}$$

Equivalently, p as a function of ρ reads:

$$p = p_c - \frac{5-\sqrt{25+32\dfrac{\rho-\rho_c}{\rho_c+p_c/c^2}}}{16}(c^2\rho_c+p_c) \tag{26}$$

One can also obtain the density profile as a function of radius using central density and pressure by substituting Eq. (23),(24) into Eq. (17). Noting that $dA^2/dp_c < 0$ and $dD^2/dp_c > 0$, one finds: $\forall r \le R, \quad p_c < c^2\rho_c/3, \quad d\rho/dp_c < 0$.

Finally, using Eq. (19) and Eq. (20):

$$A^2 = R^2\left(\frac{c^2}{GM}R-3\right), \quad D^2 = \frac{c^2}{GM}R^3 \tag{27}$$

b. Tolman VII

Assumptions

Tolman VII uses General Relativity and makes the following additional assumption:

1. A specific form is assumed for the metric function:

$$e^{-\lambda} = 1 - \frac{r^2}{D^2} + \frac{4r^4}{A^4} \tag{28}$$

Consequences

Substituting the assumed $e^{-\lambda}$ into Einstein's field equations [42, 15], and treating A, B, D, C as constants, one obtains:

$$e^{\lambda} = \frac{1}{1-r^2/D^2+4r^4/A^4} \tag{29}$$

$$e^{\nu} = B^2\left[\sin\log\left(\frac{e^{-\lambda/2}+2r^2/A^2-A^2/(4D^2)}{C}\right)^{1/2}\right]^2 \tag{30}$$

The density and pressure from the field equations are:

$$\frac{8\pi G}{c^2}\rho = \frac{3}{D^2} - \frac{20r^2}{A^4} \tag{31}$$

$$\frac{8\pi G}{c^4}p = -\frac{1}{D^2} + \frac{4r^2}{A^4} + \frac{4e^{-\lambda/2}}{A^2}\left(B^2e^{-\nu}-1\right)^{1/2} \tag{32}$$

Useful parameters

From Eq. (31), the central density (at $r = 0$) is

$$\frac{8\pi G}{c^2}\rho_c = \frac{3}{D^2} \quad\Longrightarrow\quad D^2 = \frac{3c^2}{8\pi G\rho_c} \tag{33}$$

This relation is unaffected by the treatment of the surface, since it is evaluated at the center.

Following Raghoonundun & Hobill [39], we write the density profile in the general self-bounded form

$$\rho(r) = \rho_c\left[1-\mu\left(\frac{r}{R}\right)^2\right], \qquad 0 \le \mu \le 1, \tag{34}$$

where R is the stellar boundary radius and μ is a dimensionless self-boundedness parameter controlling the surface density, $\rho(R) = \rho_c(1-\mu)$. The case $\mu = 1$ ("natural" star) corresponds to vanishing surface density, while $\mu < 1$ ("self-bound" star) allows a finite surface density, In contrast, the Chandrasekhar and Salpeter profiles vanish at a finite radius, which favours the natural case $\mu = 1$; we include $\mu < 1$ for completeness.

Matching Eq. (34) term-by-term against Eq. (31) fixes A in terms of ρ_c, R, and μ:

$$A^4 = \frac{20\,c^2 R^2}{8\pi G\,\mu\,\rho_c}, \tag{35}$$

which reduces to the earlier, $\mu = 1$ result when the surface density is required to vanish.

We stress that $\rho(R) = 0$ is *not*, in general, a boundary condition – it is only the special case $\mu = 1$ of Eq. (34). The physical condition defining the stellar surface is the vanishing of the pressure,

$$p(R) = 0, \tag{36}$$

together with continuity of the metric functions at the matching to the exterior Schwarzschild solution,

$$\begin{aligned} e^{-\lambda(R)} = e^{\nu(R)} &= 1 - \frac{2GM}{Rc^2}, \\ M &\equiv \int_0^R 4\pi r^2 \rho(r)\,dr. \end{aligned} \tag{37}$$

Because $e^{-\lambda}$ is fixed directly by the metric ansatz, one can show that $e^{-\lambda(r)} = 1 - 2Gm(r)/(rc^2)$ holds identically for every r (with $m(r) = \int_0^r 4\pi r'^2 \rho\,dr'$), so the first equality in Eq. (37) is automatically satisfied and places no restriction on R. It is Eq. (36), together with the second equality in Eq. (37), that determines the integration constants B and C appearing in e^{ν} – not the density profile itself.

Once $\rho(r)$ is fixed by D and A, $m(r)$ follows from Eq. (5) and $p(r)$ from Eq. (6) with $p(R) = 0$, without B and C (Appendix 5). We use $\mu = 0.7$–1.0.

c. Modified Vaidya–Tikekar model

The Vaidya–Tikekar model is based on a specific ansatz for the metric potential g_{rr}, motivated by the geometric property that the spatial hypersurface $t = \text{const}$, when embedded in a four-dimensional Euclidean space, has a spheroidal rather than spherical geometry. The star itself remains spherically symmetric: the parameter K controls the departure of this embedded 3-space from a 3-sphere, which is recovered for $K = 0$.

In order to generalise this model, we introduce a constant K_2, which equals 1 in the standard Vaidya–Tikekar case. This is the simplest one-parameter generalisation of the standard model. It is not unique: for $K_2 > 0$ it is only a reparametrisation of the standard model, since $D'^2 = D^2/K_2$ and $K' = K/K_2$ give $e^{\lambda} = (1 - K'r^2/D'^2)/(1 - r^2/D'^2)$, so genuinely new freedom exists only for $K_2 < 0$. We therefore regard it as a diagnostic extension rather than a physically motivated model. Regarding the usual requirements: regularity holds ($e^{\lambda(0)} = 1$, finite ρ_c, and $d\rho/dr < 0$ for $K < 0$); the energy conditions ($\rho \geq 0$, $\rho c^2 \geq p \geq 0$, $\rho c^2 + 3p \geq 0$) hold since $p/(\rho c^2) \lesssim 10^{-2}$ over the density range considered; in the classical limit the sound speed is $v_s^2 = dp/d\rho = \frac{3c^2}{4}\frac{K_2 - K}{|K|}\frac{1-u/3}{5-u}$ with $u = Kr^2/D^2 \leq 0$, so causality requires $(K_2 - K)/|K| \leq 4$ at most. In our fits K and K_2 enter only through $q = K/(K_2 - K)$; all best-fit solutions have $q < -1$, i.e. $K_2 < 0$ ($q = -30$ to -10^5), and then $v_s^2 \leq c^2/(4|q|) \lesssim 8 \times 10^{-3} c^2$, so causality holds. Restricting to $K_2 > 0$ (equivalent to the standard model) raises the density RMSD from ≈ 0.04–0.07 to ≈ 0.31–0.35 (Table 3), so the improvement comes entirely from $K_2 < 0$. Stability is not established: the fitted mass is 38–140% above the Chandrasekhar value (Fig. 9), with no turning point.

Assumptions

The model is based on General Relativity and makes the following additional assumption:

1. The metric function e^{λ} is assumed to take the

form:

$$e^{\lambda} = \frac{1 - K\dfrac{r^2}{D^2}}{1 - K_2\dfrac{r^2}{D^2}} \tag{38}$$

Consequences

Treating K and D as constants, the field equations yield:

$$\frac{8\pi G}{c^2}\rho = \frac{3(K_2 - K)}{D^2}\frac{1 - K\dfrac{r^2}{3D^2}}{\left(1 - K\dfrac{r^2}{D^2}\right)^2} \tag{39}$$

$$\frac{8\pi G}{c^4}p = \frac{1 - K_2\dfrac{r^2}{D^2}}{1 - K\dfrac{r^2}{D^2}}\left[\frac{\nu'}{r} + \frac{1}{r^2}\right] - \frac{1}{r^2} \tag{40}$$

From the definition of the mass function, $2Gm(r)/(c^2 r) = 1 - e^{-\lambda(r)}$, and the ansatz Eq. (38), which gives

$$1 - e^{-\lambda(r)} = \frac{(K_2 - K)\, r^2/D^2}{1 - K r^2/D^2}, \tag{41}$$

we obtain

$$m(r) = \frac{c^2}{2G}\frac{(K_2 - K)}{D^2}\frac{r^3}{1 - K r^2/D^2}. \tag{42}$$

Using Eq. (44) below, i.e. $(K_2 - K)/D^2 = 8\pi G\rho_c/(3c^2)$, this becomes

$$m(r) = \frac{4\pi}{3}\rho_c\frac{r^3}{1 - K\dfrac{r^2}{D^2}} \tag{43}$$

which coincides with the direct integration of $m'(r) = 4\pi\rho r^2$ using Eq. (39).

The exact value of ν is not needed for our analysis. We therefore focus on determining K and D. For computational convenience, it is useful to express the model in terms of the central density:

$$\frac{8\pi G}{c^2}\rho_c = \frac{3(K_2 - K)}{D^2} \tag{44}$$

This gives:

$$D^2 = \frac{3(K_2 - K)c^2}{8\pi G\rho_c} = \frac{3(K_2 - K)}{\alpha} \tag{45}$$

where $\alpha = 8\pi G\rho_c/c^2$ is introduced for notational convenience. Hence:

$$\rho = \rho_c\frac{1 - \alpha\dfrac{K}{9(K_2 - K)}r^2}{\left(1 - \alpha\dfrac{K}{3(K_2 - K)}r^2\right)^2} \tag{46}$$

For the central density to be positive, Eq. (44) requires $K < K_2$. The condition $d\rho/dr < 0$ inside the star gives, near the center:

$$\frac{d\rho}{dr} \underset{r\to 0}{\sim} \rho_c\,\alpha\frac{10K}{9(K_2 - K)}r$$

which requires $K < 0$.

Analyzing $d\rho/dK|_r$ at fixed ρ_c, with $u = \dfrac{\alpha K r^2}{3(K_2 - K)}$:

$$\left.\frac{d\rho}{dK}\right|_r = \frac{\rho_c\,\alpha\, r^2 K_2\,(5 - u)}{9\,(K_2 - K)^2\,(1 - u)^3} \tag{47}$$

For $K < 0$ we have $u < 0$, so $5 - u > 0$ and $1 - u > 0$. Hence $\forall K < 0$, $\forall r \geq 0$, $d\rho/dK|_r > 0$ (for $K_2 > 0$; for $K_2 < 0$ the sign reverses). One notes that $\rho(K = 0) = \rho_c$ and $\rho(K \to -\infty) \to \rho_c\dfrac{1 + \alpha r^2/9}{(1 + \alpha r^2/3)^2}$. Therefore, ρ is bounded between these two limiting profiles.

Classical limit

In the Newtonian limit $c \to \infty$, Eq. (6) reduces to:

$$\frac{dp}{dr} = -\frac{G\rho m}{r^2} \tag{48}$$

This equation can be solved using Eq. (39),

yielding:

$$p(r) - p(0) = -\frac{1}{6}\frac{K_2 - K}{K} c^2 \rho_0 \times \left(\frac{1 - \frac{Kr^2}{2D^2}}{\left(1 - \frac{Kr^2}{D^2}\right)^2} - 1 \right)$$
$$D^2 = \frac{3c^2(K_2 - K)}{8\pi\rho_0 G} \tag{49}$$

For the star to have a finite radius, one requires $p(R) = 0$ with $R > 0$, which imposes:

$$p(0) \in \left[0, \frac{K - K_2}{K}\frac{c^2\rho_0}{6}\right] \tag{50}$$

To express $p(0)$ as a function of the total radius and total mass, one uses the mass relation Eq. (43) together with the condition $p(R) = 0$:

$$R^2 = -\frac{D^2}{K}\frac{\sqrt{2\alpha + 9/4} - (2\alpha + 3/2)}{2\alpha + 2}$$
$$\alpha = \frac{6p(0)K}{c^2\rho(0)(K_2 - K)} \tag{51}$$

Inverting this relation and setting $x = -KR^2/D^2$:

$$\alpha = \frac{6p(0)K}{c^2\rho(0)(K_2 - K)} = -\frac{x(2x+3)}{2(x+1)^2} \tag{52}$$

4. Results and Discussion

The central question is now whether the field equation models are compatible with the Chandrasekhar or Salpeter equations of state. We compare the density and pressure profiles as functions of radius, the equation of state, and the total mass–radius relation.

a. Equation of state

Figure 1 compares all models at the same ρ_c and p_c. None of them follows the Chandrasekhar and Salpeter equations of state, which are nearly identical. Tolman IV and the standard Vaidya–Tikekar model cover almost no density range, the modified Vaidya–Tikekar model stops at $\rho_s \simeq 0.03\,\rho_c$, and Tolman VII is too steep: for $\mu = 1$ its effective index $d\ln p/d\ln\rho$ is 2.3–2.0, against 1.35–1.45 for Chandrasekhar, and $p_{\mathrm{T7}}/p_{\mathrm{Ch}} = 0.48, 0.12, 0.03$ at $\rho/\rho_c = 0.5, 0.1, 0.01$.

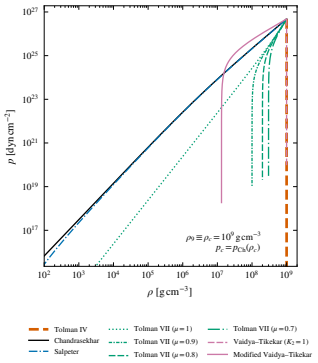


Figure 1 - $p(\rho)$ inside a representative star with $\rho_c = 10^9\,\mathrm{g\,cm^{-3}}$ and p_c equal to the Chandrasekhar value ($A/Z = 2$). Each curve is the relation along the radius of one star, not a universal equation of state. The Vaidya–Tikekar curve is hidden behind the Tolman IV one: both end almost vertically at $\rho \simeq \rho_c$ (surface density within 0.4% of ρ_c) and lie on the right edge of the frame.

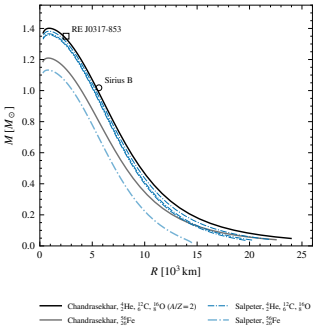


Figure 2 - Mass–radius relation for $^4_2$He, $^{12}_6$C, $^{16}_8$O, $^{56}_{26}$Fe using the Chandrasekhar and Salpeter equations of state for a range of central densities 10^4–$10^{12}\,\mathrm{g\cdot cm^{-3}}$.

b. Quantum statistical mass–radius relations

As predicted by Eq. (10), for equal mass the radius of the star is smaller in the Salpeter model than in Chandrasekhar's, because the pressure is lower at equal Fermi momentum. We also show Sirius B [43], 40 Eridani B [44] and RE J0317-853 [45]. All three lie above the zero-temperature curves, which is expected from the finite-temperature and envelope effects neglected here (and, for RE J0317-853, from rotation and a strong magnetic field).

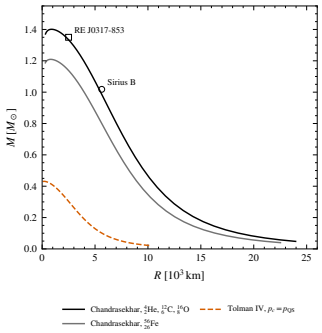


Figure 3 - Mass–radius relation for Tolman IV using the same central density and pressure as for the Chandrasekhar model. pQS stands for "pressure from quantum statistical equations of state".

c. Pressure versus density

The equation of state for the Chandrasekhar and Salpeter models is readily obtained from Eq. (4). One also notes that $\forall y > 0.2$, $|p_{\text{Salpeter}}(y)/p_{\text{Chandrasekhar}}(y)| \geq 0.7$.

A key observation is that the function $p(\rho)$ (the equation of state) in Eq. (26) is concave (negative second derivative), whereas in Eq. (4) it is strictly convex (positive second derivative). The Tolman IV model is therefore fundamentally incompatible with quantum statistical equations of state such as those of Chandrasekhar or Salpeter.

d. Mass versus radius

In this section, we compute the total mass–radius relation and assess whether the Tolman IV model is globally consistent with quantum statistical predictions.

The mass–radius relation for quantum statistical models is already established; we therefore carry it out for Tolman IV only. Since the quantum statistical equations are solved using ρ_c as the initial condition, we proceed likewise. However, since two equations are needed to determine A and D, we also use the central pressure p_c from quantum statistics. And we obtain this pressure by inverting Eq. (3) and by plugging in Eq. (4). The resulting mass–radius diagram, computed in Python, is shown below.

The Tolman IV curve lies well below the Chandrasekhar in Figure 3, indicating that the model compactifies the star excessively. Moreover, the maximum mass is around $0.4\,M_\odot$, far below the Chandrasekhar limit ($\approx 1.4\,M_\odot$). This constitutes a second confirmation of the incompatibility between Tolman IV and quantum statistical equations of state.

Table 1 – Central parameters that Tolman IV would need to reproduce the Chandrasekhar mass–radius relation ($A/Z = 2$). Here ρ_c^{QS} and p_c^{QS} are the quantum statistical values, and A^2 is obtained from Eq. (27).

ρ_c^{QS} (g cm^{-3})	p_c^{QS} (dyn cm^{-2})	A^2 (cm^2)	$\rho_{c,\text{T4}}$ (g cm^{-3})	$p_{c,\text{T4}}$ (dyn cm^{-2})
10^5	6.41×10^{20}	1.99×10^{23}	1.61×10^{4}	9.59×10^{19}
10^7	8.36×10^{23}	2.94×10^{21}	1.09×10^{6}	8.23×10^{22}
10^9	4.81×10^{26}	7.41×10^{19}	4.33×10^{7}	1.57×10^{25}
10^{11}	2.26×10^{29}	1.34×10^{18}	2.38×10^{9}	3.40×10^{27}

Even if one were to tune the central density and pressure so that the Tolman IV mass–radius relation matches the Chandrasekhar curve, the required central values would differ strongly from the quantum statistical ones. To quantify this, we insert each Chandrasekhar pair (M,R) with $A/Z = 2$ into Eq. (27) and obtain the effective central values $\rho_{c,\text{T4}}$ and $p_{c,\text{T4}}$ from Eqs. (21) and (22); selected results are listed in Table 1.

The mass–radius relations can be made to coincide, but only with effective central values far below the quantum statistical ones: $\rho_{c,\text{T4}}$ is only about 2–16% of ρ_c^{QS}, and $p_{c,\text{T4}}$ about 1.5–15% of p_c^{QS}, over $\rho_c^{\text{QS}} = 10^5$–$10^{11}\ \text{g cm}^{-3}$.

e. Density and pressure profiles

Tolman IV

Fixing the total mass and radius in accordance with the Chandrasekhar mass–radius relation for average atomic mass number per electron $A/Z = 2$, one can extract the corresponding central density and pressure from the quantum statistical equations. Substituting Eq. (27) into Eq. (17) then yields the Tolman IV density profile. The results are shown in Figure 4,5.

These figures confirm, across a wide range of total mass and radius, that the Tolman IV model is entirely unable to reproduce the equation of state,

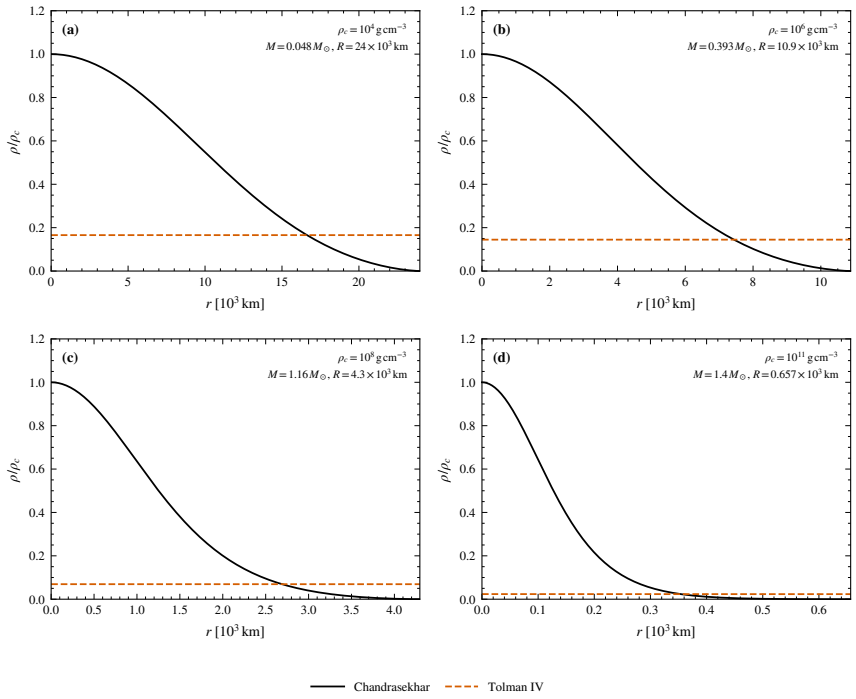


Figure 4 - Density profiles for the Tolman IV and Chandrasekhar models, obtained by fixing the total mass and radius corresponding to central densities $\rho_c = 10^4$–10^{12} g cm^{-3}.

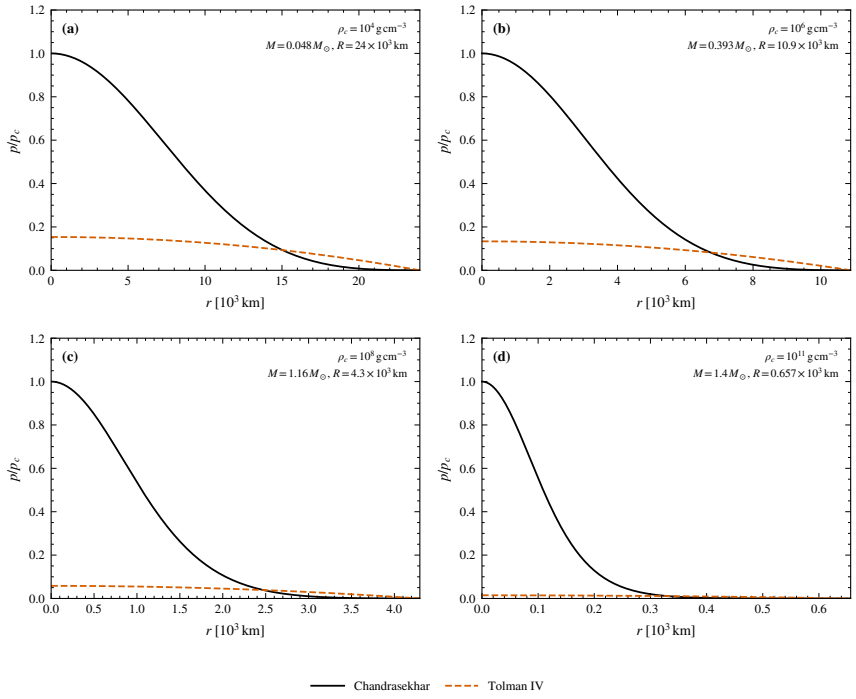


Figure 5 - Pressure profiles for the Tolman IV and Chandrasekhar models, obtained by fixing the total mass and radius corresponding to central densities $\rho_c = 10^4$–10^{12} g cm^{-3}.

the mass–radius relation, or the pressure and density profiles predicted by quantum statistical models.

Tolman VII

The Tolman VII solution is an exact interior solution of the Einstein field equations charac-

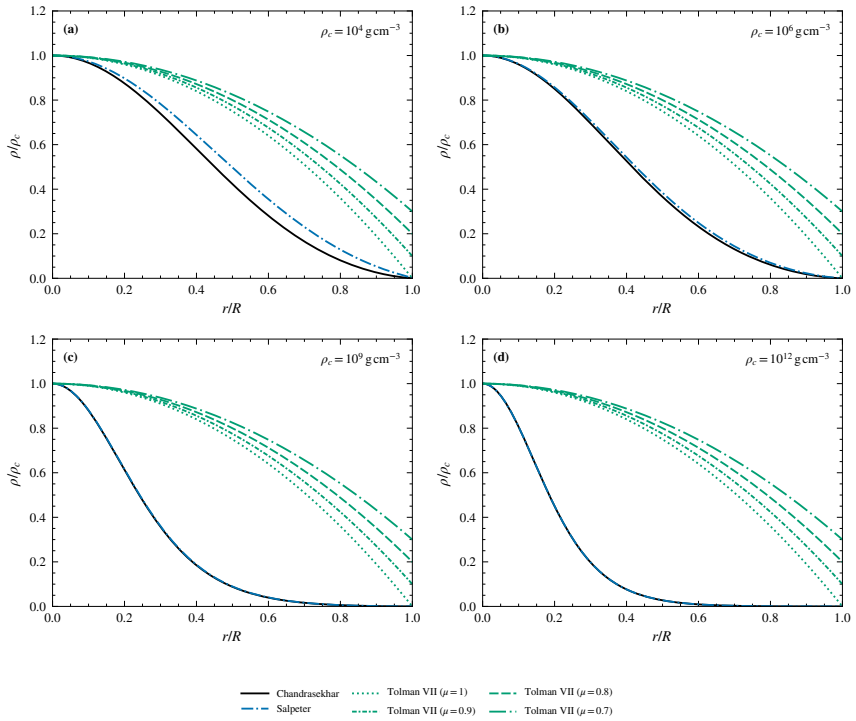


Figure 6 - Normalised density profiles ρ/ρ_c vs r/R for the Tolman VII family ($\mu = 1.0, 0.9, 0.8, 0.7$) compared with the Chandrasekhar and Salpeter profiles, at four central densities. The Tolman VII curves lie strictly above both quantum-statistical profiles at every interior radius for the entire range of μ considered, with the discrepancy growing with increasing ρ_c.

terised by a parabolic density profile, Eq. (34), controlled by the self-boundedness parameter μ [39]. It is widely used as an analytic approximation to compact stellar structure because it admits closed-form expressions for the metric and pressure, avoiding the need to numerically integrate the Tolman-Oppenheimer-Volkoff equations [41]. However, the profile is purely geometric in origin: it is not derived from any microphysical equation of state, and so its validity for a given class of star is not guaranteed *apriori*. For white dwarfs, the relevant equations of state are the Chandrasekhar and Salpeter models, both of which describe pressure support from a degenerate, relativistic electron gas, with Salpeter additionally incorporating Coulomb lattice corrections. To test whether the Tolman VII ansatz is a reasonable structural surrogate for these microphysically motivated models, we compare the shape of the Tolman VII parabolic profile, for a representative range of μ, directly against the shapes of the Chandrasekhar and Salpeter density profiles.

We compare the Tolman VII profile Eq. (34), for $\mu = 1.0, 0.9, 0.8, 0.7$, with the Chandrasekhar and Salpeter profiles at four central densities $\rho_c = 10^4$-10^{12} $\mathrm{g\,cm^{-3}}$ by normalizing both axes, so that only the shape is compared independently of scale. Each profile is rescaled as ρ/ρ_c against r/R, where R is the stellar boundary radius, taken equal to the Chandrasekhar radius at each central density. This normalization fixes the central point of every curve to $\rho/\rho_c = 1$ at $r/R = 0$; the Tolman VII family additionally satisfies $\rho/\rho_c = 1 - \mu$ at $r/R = 1$, reducing to zero only in the natural case $\mu = 1$.

Table 2 quantifies this discrepancy for the two extremal values of the self-boundedness parameter, $\mu = 1.0$ (natural star) and $\mu = 0.7$; intermediate values of μ produce RMSD values that fall monotonically between these two bounds. In every case, the RMS deviation increases with central density, growing by a factor of roughly 1.7–2.8 between $\rho_c = 10^4$ and 10^{12} $\mathrm{g\,cm^{-3}}$, confirming that the mismatch between the Tolman

Table 2 – Root-mean-square deviation (RMSD) of the normalised Tolman VII density profile, $\rho_{T7}(r)/\rho_c = 1-\mu(r/R)^2$, from the normalised Chandrasekhar and Salpeter profiles, evaluated at each central density for the two extremal self-boundedness values $\mu = 1.0$ (natural star) and $\mu = 0.7$. RMSD is defined as $\left[\frac{1}{N}\sum_i \left(\frac{\rho_{T7}(r_i)}{\rho_c} - \frac{\rho_{EOS}(r_i)}{\rho_c}\right)^2\right]^{1/2}$, with r_i sampled uniformly over $[0,R]$.

ρ_c [g cm^{-3}]	RMSD (Chandrasekhar)		RMSD (Salpeter)	
	$\mu = 1.0$	$\mu = 0.7$	$\mu = 1.0$	$\mu = 0.7$
10^4	0.2372	0.3469	0.1882	0.3009
10^6	0.2709	0.3773	0.2594	0.3666
10^9	0.4547	0.5441	0.4534	0.5429
10^{12}	0.5217	0.6050	0.5215	0.6048

VII geometric ansatz and the microphysical equations of state is not merely qualitative but grows systematically with increasing central density. For every value of μ examined, the Tolman VII profile lies strictly above both quantum-statistical profiles for all $0 < r/R < 1$. The quantum-statistical profiles fall off comparatively steeply, with density dropping rapidly through the stellar interior and approaching zero sharply near the boundary, whereas the Tolman VII profiles decrease far more gradually, retaining a disproportionately high density fraction throughout the outer layers; decreasing μ raises the surface density $\rho(R) = \rho_c(1-\mu)$ and moves the family *further* above the quantum-statistical curves (Table 2), but does not remove the mismatch in the bulk of the star, nor bring the profile into agreement with the steep near-boundary falloff of the Chandrasekhar and Salpeter curves. This mismatch is therefore structural rather than an artifact of a single parameter choice: the parabolic form of the Tolman VII profile, for any $\mu \in [0.7, 1.0]$, cannot reproduce the steeper falloff characteristic of the quantum-statistical equation of state. Moreover, the magnitude of the discrepancy increases systematically with ρ_c, indicating that the Tolman VII approximation becomes progressively worse as the star approaches the relativistic, high-density regime, independently of μ. The Tolman VII solution is therefore incompatible with the quantum-statistical equation of state across the entire white dwarf density range and the physically reasonable range of self-boundedness, and should not be used as a structural substitute for microphysically derived equations of state in this context.

Vaidya–Tikekar

Recall that the standard Vaidya–Tikekar model corresponds to $K_2 = 1$ in Eq. (46). The most direct test of incompatibility consists in analysing this equation. Using Eq. (47), it suffices to compare the density profile in the limiting case $K \to -\infty$ with the Chandrasekhar prediction at fixed central density. If this limiting profile lies strictly above the Chandrasekhar curve for all admissible radii, then no choice of $K < 0$ can reproduce the quantum statistical equation of state. The results for central densities $\rho_c = 10^4$–10^{12} g cm^{-3} are shown in Figure 7.

The Vaidya–Tikekar profile lies strictly above the Chandrasekhar prediction in all cases. We therefore conclude that the standard Vaidya–Tikekar model is incompatible with the Chandrasekhar equation of state.

We then introduce the parameter K_2 from Eq. (46) and seek the best-fit values of K, K_2, and ρ_c that minimise the discrepancy between the Vaidya–Tikekar and Chandrasekhar density profiles. Using Python to optimise the modified model over a range of central densities 10^4–10^{12} g cm^{-3}, using the interpolated density parameters and fixing the total stellar radius to that given by the Chandrasekhar equation of state:

- Using the classical hydrostatic equation and the analytical pressure expression Eqs. (49)–(52).
- Solving the TOV equations numerically.

As we can see in Figures 7 and 8, the density fit improves near the core as the central density increases. However, from the midpoint to the stellar surface the agreement deteriorates significantly, because the modified Vaidya–Tikekar density profile cannot vanish at a finite radius. This structural limitation degrades the quality of

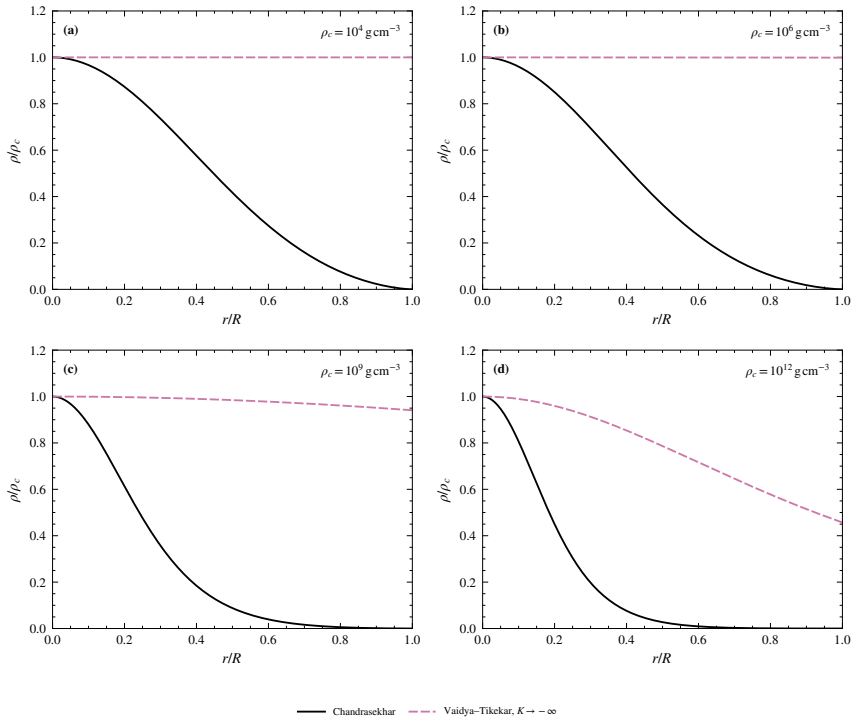


Figure 7 - Density profiles for the Vaidya–Tikekar model in the limit $K \to -\infty$ and for the Chandrasekhar model, at fixed central density.

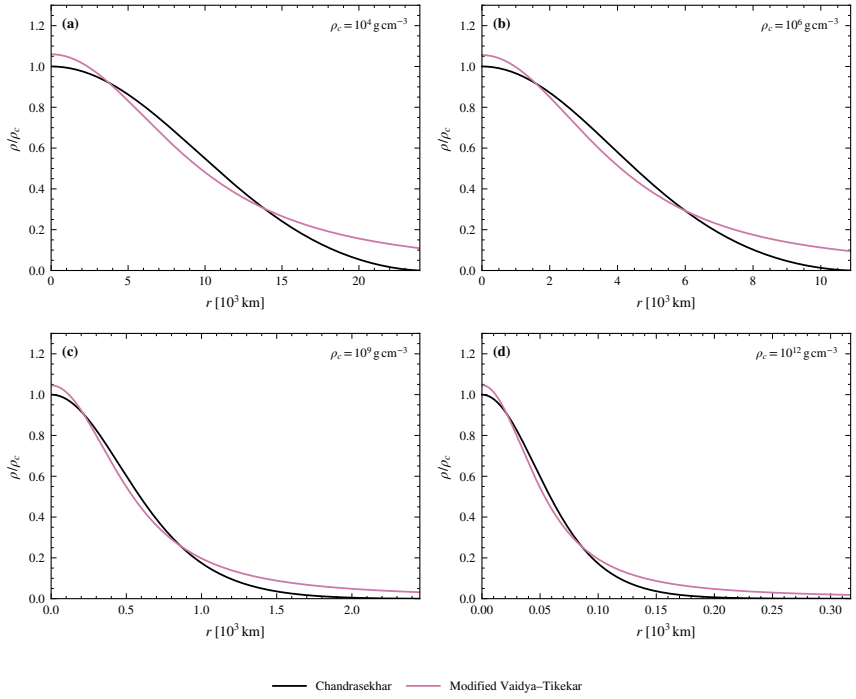


Figure 8 - Density profiles for the modified Vaidya–Tikekar model, fitted to the Chandrasekhar density profile. The range of central densities used is 10^4–10^{12} g $\cdot$ cm^{-3}.

the pressure fit accordingly. While the modified model outperforms both Tolman IV and the standard Vaidya–Tikekar model, the fit remains unsatisfactory. The mass–radius relation obtained from the interpolated parameters is shown Figure 9.

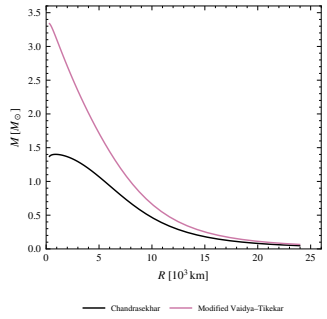


Figure 9 - Mass–radius relation using the Chandrasekhar equation of state and the modified Vaidya–Tikekar model.

Table 3 – RMSD of the normalised density profile with respect to Chandrasekhar ($A/Z = 2$), $r \in [0, R_{\rm Ch}]$, and mass ratio of the fitted modified Vaidya–Tikekar star at $R = R_{\rm Ch}$.

ρ_c [g cm^{-3}]	VT ($K \to -\infty$)	mod. VT $K_2 > 0$	mod. VT free	$M_{\rm VT}/M_{\rm Ch}$
10^4	0.644	0.351	0.068	1.38
10^6	0.666	0.351	0.062	1.41
10^9	0.779	0.344	0.040	1.90
10^{12}	0.601	0.314	0.036	2.42

The relative mass error of the fitted model is already $\approx 40\%$ at $\rho_c = 10^4$–10^6 g cm^{-3} and reaches 90–140% at 10^9–10^{12} g cm^{-3} (Table 3), so the fit is poor at all central densities and worst at high densities (small radii). Two effects are responsible. First, the Vaidya–Tikekar density profile never vanishes, whereas the Chandrasekhar profile goes to zero at a finite radius, so the outer layers carry excess mass. Second, at low densities the Vaidya–Tikekar profile passes from below to above the Chandrasekhar profile, so part of the error cancels upon integration, but this cancellation is incomplete and a mass excess of $\approx 40\%$ remains.

f. Comparison with observations

We confront the models with two white dwarfs having independent dynamical masses and precise radii: Sirius B ($M = 1.018 \pm 0.011\,M_\odot$, $R = 0.008098\,R_\odot$) [43] and 40 Eridani B ($M = 0.573 \pm 0.018\,M_\odot$, $R = 0.01308 \pm 0.00020\,R_\odot$) [44]. Larger Gaia-based samples are a natural extension, but their radii rely on atmosphere models, so we restrict ourselves to these benchmarks. At the observed masses, the zero-temperature Chandrasekhar relation ($A/Z = 2$) underestimates the radii by 4.5% and 2.0% (Table 4), in the direction expected from the finite-temperature and envelope effects neglected here. Tolman IV, by contrast, cannot reach either mass: its maximum is $0.43\,M_\odot$, and at the observed radii it gives only 0.10 and $0.04\,M_\odot$.

Table 4 – Observed white dwarfs versus model predictions ($p_c = p_{\rm Ch}(\rho_c)$ for Tolman IV).

Star	M [$M_\odot$]	$R_{\rm obs}$ [km]	$R_{\rm Ch}(M)$ [km]	Dev.	$M_{\rm T4}(R_{\rm obs})$ [$M_\odot$]
Sirius B	1.018	5634	5392	+4.5%	0.10
40 Eri B	0.573	9100	8919	+2.0%	0.04

5. CONCLUSIONS

We have carried out a systematic comparison of three exact general relativistic interior solutions — Tolman IV, Tolman VII, and Vaidya–Tikekar — against the quantum statistical equations of state appropriate for white dwarf interiors, namely the Chandrasekhar and Salpeter models. Our analysis proceeded along three complementary lines of evidence: the curvature of the equation of state, the mass–radius diagram, and the interior density and pressure profiles.

The incompatibility of each model with quantum statistical equations of state manifests in a distinct way. For Tolman IV, the equation of state is concave, in direct contradiction with the strict convexity of both the Chandrasekhar and Salpeter equations of state across the entire white dwarf density range $\rho_c = 10^4$–10^{12} g cm^{-3}. This curvature mismatch is analytic and independent of the model parameters, and is confirmed numerically by the mass–radius diagram, which yields a maximum mass of approximately $0.4\,M_\odot$ — far below the observed Chandrasekhar limit — and by density and pressure profiles that deviate substantially from the quantum statistical predictions at all central densities considered. The comparison with Sirius B and 40 Eridani B (Table 4) points the same way: the Chandrasekhar relation reproduces their radii to within 2–5%,

whereas Tolman IV cannot reach either mass. For Tolman VII, the fixed parabolic shape of the density profile is structurally incompatible with the Chandrasekhar and Salpeter predictions: the normalised profile lies strictly above both quantum statistical curves at every interior radius for the full physically reasonable range of the self-boundedness parameter μ, and this discrepancy cannot be removed by adjusting the model parameters within the range considered. For the Vaidya–Tikekar model, the monotonicity of the density profile in the geometric parameter K allows one to reduce the problem to its limiting case $K \to -\infty$, which still lies strictly above the Chandrasekhar prediction for all admissible radii and all central densities examined. Introducing the additional free parameter K_2 improves the density fit near the core, particularly at high central densities, but the modified model inherits the fundamental defect that its density profile cannot vanish at a finite radius. This structural limitation causes the fit to deteriorate systematically near the stellar surface and at high densities, where it also results in a poor mass–radius relation.

Part of the explanation lies in the very different gravitational regimes occupied by white dwarfs and neutron stars. Typical white dwarfs satisfy $GM/(Rc^2) \sim 10^{-4}$, placing them much closer to the Newtonian limit than neutron stars, for which this ratio is of order 0.1–0.3. Exact relativistic interior solutions such as Tolman IV, Tolman VII, and Vaidya–Tikekar were constructed, and have been validated, in the strong-field regime characteristic of neutron stars; their metric ansätze encode curvature properties tuned to that regime rather than to the near-Newtonian, strictly convex equation of state of a degenerate electron gas. This raises the broader question of whether exact relativistic interior solutions are expected to offer significant physical insight for weakly relativistic objects such as white dwarfs in the first place, independently of the specific ansatz chosen.

The common origin of these failures lies in a fundamental difference between the microphysics of white dwarfs and neutron stars. Geometric interior solutions such as Tolman IV, Tolman VII, and Vaidya–Tikekar were developed and validated in the context of compact objects with concave equations of state at supranuclear densities — a regime characteristic of neutron stars. White dwarfs, by contrast, are governed by a strictly convex electron degeneracy pressure over their entire density range, and their density profiles vanish at a finite radius. Neither property can be accommodated by any of the geometric models considered here without modifying the underlying ansatz. Our results therefore delineates a clear boundary, for the three models examined here, between the class of compact objects for which they are physically appropriate and the white dwarf regime, where a microphysical treatment of the equation of state is indispensable. We stress that this conclusion is restricted to Tolman IV, Tolman VII, and Vaidya–Tikekar; numerous other exact interior solutions exist in the literature (e.g. Buchdahl, Heintzmann, Durgapal, Finch–Skea, Adler, Kuchowicz, Pant–Sah, and others) whose compatibility with white dwarf matter has not been tested here and remains an open question. Extending analytical interior solutions to white dwarfs would require either constructing new ansätze specifically designed to reproduce convex equations of state with a finite stellar surface, or coupling the geometric metric directly to the quantum statistical equation of state rather than treating the two independently. Both directions remain open for future work, as does the question of whether thermal corrections, magnetic fields, or rotation could alter the compatibility landscape in any significant way.

It would be interesting to study alternative models of white dwarf stars involving dark matter distribution in the their cores and surroundings in analogy with [46, 47, 48, 49, 50, 51, 52]. However this task is out of the scope of the present work and will be considered in future studies.

Author Contributions: Conceptualization, V.O. and M.S.M.; methodology, V.O. and M.S.M.; software, V.O. and M.S.M.; validation, V.O. and M.S.M.; formal analysis, B.N. and A.A.; investigation, V.O., M.S.M., B.N. and A.A.;

writing—original draft preparation, V.O. and M.S.M.; writing—review and editing, B.N. and A.A.; visualization, V.O. and M.S.M. All authors have read and agreed to the published version of the manuscript.

ACKNOWLEDGMENTS

NB and AA acknowledge the support by the Ministry of Science and Higher Education of the Republic of Kazakhstan, grant IRN AP23490322.

APPENDIX

Exterior and interior solutions

Here we consider matching conditions between exterior and interior solutions. The line element for global solution is given by

$$\begin{aligned} ds^2 = &-e^{\nu(r)}dt^2 + e^{\lambda(r)}dr^2 \\ &+ r^2 d\theta^2 + r^2 \sin^2\theta\, d\phi^2 . \end{aligned} \tag{53}$$

For the exterior solution $r \geq R$ we have the Schwarzschild vacuum solution

$$\begin{aligned} e^{\nu(r)} &= 1 - \frac{2M}{r}, \\ e^{\lambda(r)} &= \left(1 - \frac{2M}{r}\right)^{-1} \end{aligned} \tag{54}$$

For the interior solution $r \leq R$ we have Tolman IV solution expressed in terms of the total mass and radius R

$$\begin{aligned} e^{\nu(r)} &= \left(1 - \frac{3M}{R}\right)\left(1 + \frac{Mr^2}{R^2(R-3M)}\right) \\ &= 1 - \frac{3M}{R} + \frac{Mr^2}{R^3}, \end{aligned} \tag{55}$$

$$\begin{aligned} e^{\lambda(r)} &= \frac{1 + \dfrac{2Mr^2}{R^2(R-3M)}}{\left(1 - \frac{Mr^2}{R^3}\right)\left(1 + \frac{Mr^2}{R^2(R-3M)}\right)} \\ &= \left[\frac{\left(1 - \frac{Mr^2}{R^3}\right)\left(1 - \frac{M(3R^2-r^2)}{R^3}\right)}{\left(1 - \frac{M(3R^2-2r^2)}{R^3}\right)}\right]^{-1} . \end{aligned} \tag{56}$$

As one may notice, both solutions match smoothly on the surface of the compact object when $r = R$. Moreover, unlike the function $e^{\lambda(r)}$, the derivatives of the function $e^{\nu(r)}$ also match smoothly at the boundary $r = R$.

Pressure–density relation

Tolman VII. With $\rho = \rho_c[1 - \mu(r/R)^2]$, Eq. (5) gives $m = 4\pi\rho_c(r^3/3 - \mu r^5/5R^2)$. Eq. (6) is then first order in p, solved with $p(R) = 0$; R follows from $p(0) = p_c$.

Vaidya–Tikekar. With $s = Kr^2/D^2$, $\kappa = (K_2 - K)/K$ and Eqs. (46),(49):

$$\frac{d^2p}{d\rho^2} = \frac{3\kappa c^2(1-s)^3}{2\rho_c(5-s)^3} < 0 \quad (\kappa < 0,\ s \leq 0). \tag{57}$$

REFERENCES

[1] Chandrasekhar, S. "The maximum mass of ideal white dwarfs." *The Astrophysical Journal* 74 (1931): 81–82. https://doi.org/10.1086/143324

[2] Shapiro, S. L. and S. A. Teukolsky. *Black Holes, White Dwarfs, and Neutron Stars: The Physics of Compact Objects*. New York: Wiley-Interscience, 1983.

[3] Althaus, L. G., A. H. Córsico, J. Isern, and E. García-Berro. "Evolutionary and pulsational properties of white dwarf stars." *The Astronomy and Astrophysics Review* 18, no. 4 (2010): 471–566. https://doi.org/10.1007/s00159-010-0033-1

[4] Chandrasekhar, S. "The highly collapsed configurations of a stellar mass (second paper)." *Monthly Notices of the Royal Astronomical Society* 95, no. 3 (1935): 207–225. https://doi.org/10.1093/mnras/95.3.207

[5] Chandrasekhar, S. *An Introduction to the Study of Stellar Structure*. Chicago: University of Chicago Press, 1939.

[6] Salpeter, E. E. "Energy and pressure of a zero-temperature plasma." *The Astrophysical Journal* 134 (1961): 669–682. https://doi.org/10.1086/147194

[7] Zapolsky, H. S. and E. E. Salpeter. "The mass-radius relation for cold spheres of low mass." *The Astrophysical Journal* 158 (1969): 809–813. https://doi.org/10.1086/150240

[8] Hamada, T. and E. E. Salpeter. "Models for zero-temperature stars." *The Astrophysical Journal* 134 (1961): 683–698. https://doi.org/10.1086/147195

[9] Boshkayev, K. "Spin-up and spin-down evolution in general relativistic rotating white dwarfs." *International Journal of Mathematics and Physics* 4, no. 1 (2013): 62–66. https://ijmph.kaznu.kz/index.php/kaznu/article/view/55

[10] Boshkayev, K. "Non-rotating and slowly rotating stars in classical physics." *International Journal of Mathematics and Physics* 5, no. 1 (2014): 69–80. https://doi.org/10.26577/2218-7987-2014-5-1-69-80

[11] Boshkayev, K., J. Rueda, R. Ruffini, B. Zhami, Z. Kalymova, and G. Balgimbekov. "Non-rotating and slowly rotating white dwarfs in classical physics." *Physical Sciences and Technology* 2, no. 1 (2016):. https://phst.kaznu.kz/index.php/journal/article/view/64

[12] Boshkayev, K., J. A. Rueda, and M. Muccino. "Evolution of isolated white dwarfs." *International Journal of Mathematics and Physics* 5, no. 2 (2014): 33–66. https://doi.org/10.26577/2218-7987-2014-5-2-33-36

[13] Boshkayev, K., O. Luongo, M. Muccino, and Q. H. "Static and rotating white dwarf stars at finite temperatures." *International Journal of Mathematics and Physics* 12, no. 2 (2021): 61–69. https://doi.org/10.26577/ijmph.2021.v12.i2.07

[14] Schwarzschild, K. "Über das gravitationsfeld einer kugel aus inkompressibler flüssigkeit nach der einsteinschen theorie." *Sitzungsberichte der Königlich Preussischen Akademie der Wissenschaften* (1916): 424–434.

[15] Tolman, R. C. "Static solutions of einstein's field equations for spheres of fluid." *Physical Review* 55, no. 4 (1939): 364–373. https://doi.org/10.1103/PhysRev.55.364

[16] Lattimer, J. M. and M. Prakash. "Neutron star structure and the equation of state." *The Astrophysical Journal* 550, no. 1 (2001): 426–442. https://doi.org/10.1086/319702

[17] Delgaty, M. S. R. and K. Lake. "Physical acceptability of isolated, static, spherically symmetric, perfect fluid solutions of einstein's equations." *Computer Physics Communications* 115 (1998): 395–415. https://doi.org/10.1016/S0010-4655(98)00130-1

[18] Vaidya, P. C. and R. Tikekar. "Exact relativistic model for a superdense star." *Journal of Astrophysics and Astronomy* 3 (1982): 325–334. https://doi.org/10.1007/BF02714870

[19] Tikekar, R. "Exact model for a relativistic star." *Journal of Mathematical Physics* 31, no. 10 (1990): 2454–2458. https://doi.org/10.1063/1.528851

[20] Tikekar, R. and K. Jotania. "A relativistic two-parameter core-envelope model of compact stars." *Gravitation and Cosmology* 15, no. 2 (2009): 129–133. https://doi.org/10.1134/S0202289309020042

[21] Mukherjee, S., B. C. Paul, and N. K. Dadhich. "Relativistic star solutions in higher dimensions with anisotropic pressure." *Classical and Quantum Gravity* 14 (1997): 3475–3490. https://doi.org/10.1088/0264-9381/14/12/027

[22] Sharma, R., S. Mukherjee, and S. D. Maharaj. "General solution for a class of static charged spheres." *General Relativity and Gravitation* 33, no. 6 (2001): 999–1009. https://doi.org/10.1023/A:1010272130226

[23] Lattimer, J. M. and M. Prakash. "Neutron star observations: Prognosis for equation of state constraints." *Physics Reports* 442 (2007): 109–165. https://doi.org/10.1016/j.physrep.2007.02.003

[24] Özel, F. and P. Freire. "Masses, radii, and the equation of state of neutron stars." *Annual Review of Astronomy and Astrophysics* 54 (2016): 401–440. https://doi.org/10.1146/annurev-astro-081915-023322

[25] Boshkayev, K., J. A. Rueda, and M. Muccino. "Theoretical and observational constrainhts on the mass-radius relations of neutron stars." *Physical Sciences and Technology* 3, no. 1 (2017):. https://phst.kaznu.kz/index.php/journal/article/view/89

[26] Bowers, R. L. and E. P. T. Liang. "Anisotropic spheres in general relativity." *The Astrophysical Journal* 188 (1974): 657–665. https://doi.org/10.1086/152760

[27] Herrera, L. and N. O. Santos. "Local anisotropy in self-gravitating systems." *Physics Reports* 286, no. 2 (1997): 53–130. https://doi.org/10.1016/S0370-1573(96)00042-7

[28] Mak, M. K. and T. Harko. "Anisotropic stars in general relativity." *Proceedings of the Royal Society of London A* 459, no. 2030 (2003): 393–408. https://doi.org/10.1098/rspa.2002.1014

[29] de Carvalho, S. M., M. Rotondo, J. A. Rueda, and R. Ruffini. "Relativistic Feynman-Metropolis-Teller treatment at finite temperatures." *Phys. Rev. C* 89 (2014): 015801. https://doi.org/10.1103/PhysRevC.89.015801

[30] Boshkayev, K., J. A. Rueda, R. Ruffini, B. Zhami, Z. Kalymova, and G. Balgimbekov. "Mass-radius relations of white dwarfs at finite temperatures." *arXiv e-prints* (2016):. https://arxiv.org/abs/1604.02391

[31] Hartle, J. B. "Slowly Rotating Relativistic Stars. I. Equations of Structure." *The Astrophysical Journal* 150 (1967): 1005.

[32] Hartle, J. B. and K. S. Thorne. "Slowly Rotating Relativistic Stars. II. Models for Neutron Stars and Supermassive Stars." *The Astrophysical Journal* 153 (1968): 807.

[33] Suliyeva, G. B., K. Boshkayev, G. Nurbakyt, H. Quevedo, A. S. Taukenova, A. T. Tlemissov, Z. A. Tlemissova, and A. Urazalina. "Adiabatic theory of motion of bodies in the hartle-thorne spacetime." *International Journal of Mathematics and Physics* 13, no. 1 (2022): 82–90. https://ijmph.kaznu.kz/index.php/kaznu/article/view/460

[34] Boshkayev, K., O. Luongo, M. Muccino, and H. Quevedo. "Static and rotating white dwarf stars at finite temperatures." *International Journal of Mathematics and Physics* 12, no. 2 (2021): 61–69. https://ijmph.kaznu.kz/index.php/kaznu/article/view/405

[35] Bera, P. and D. Bhattacharya. "Mass-radius relation of strongly magnetized white dwarfs: dependence on field geometry, GR effects and electrostatic corrections to the EOS." *Monthly Notices of the Royal Astronomical Society* 456 (2016): 3375. https://doi.org/10.1093/mnras/stv2823

[36] Muratkhan, A., A. Taukenova, S. Toktarbay, and H. Quevedo. "Rotation-Induced Effective Anisotropy in White Dwarfs as a Newtonian Benchmark with Relativistic Scale Assessment." *arXiv e-prints* (2026): arXiv:2604.27956. https://doi.org/10.48550/arXiv.2604.27956

[37] Lindblom, L. "The relativistic inverse stellar structure problem." *AIP Conference Proceedings* 1577 (2014): 153. https://doi.org/10.1063/1.4861951

[38] Baym, G., C. Pethick, and P. Sutherland. "The ground state of matter at high densities: Equation of state and stellar models." *The Astrophysical Journal* 170 (1971): 299–317. https://doi.org/10.1086/151216

[39] Raghoonundun, A. M. and D. W. Hobill. "Possible physical realizations of the Tolman VII solution." *Phys. Rev. D* 92 (2015): 124005. https://doi.org/10.1103/PhysRevD.92.124005

[40] Demissenova, D., N. Beissen, K. Boshkayev, and H. Quevedo. "Thermodynamic acceptability of spherically symmetric perfect-fluid solutions in general relativity." *arXiv e-prints* (2026): arXiv:2605.21990. https://arxiv.org/abs/2605.21990

[41] Oppenheimer, J. R. and G. M. Volkoff. "On massive neutron cores." *Physical Review* 55, no. 4 (1939): 374–381. https://doi.org/10.1103/PhysRev.55.374

[42] Misner, C. W., K. S. Thorne, and J. A. Wheeler. *Gravitation*. San Francisco: W. H. Freeman, 1973.

[43] Bond, H. E., G. H. Schaefer, R. L. Gilliland, J. B. Holberg, B. D. Mason, I. W. Lindenblad, M. Seitz-McLeese, W. D. Arnett, P. Demarque, F. Spada, P. A. Young, M. A. Barstow, M. R. Burleigh, and D. Gudehus. "The sirius system and its astrophysical puzzles: Hubble space telescope and ground-based astrometry." *The Astrophysical Journal* 840 (2017): 70. https://doi.org/10.3847/1538-4357/aa6af8

[44] Bond, H. E., P. Bergeron, and A. Bédard. "Astrophysical implications of a new dynamical mass for the nearby white dwarf 40 eridani b." *The Astrophysical Journal* 848 (2017): 16. https://arxiv.org/abs/1709.00478

[45] Barstow, M. A., S. Jordan, D. O'Donoghue, M. R. Burleigh, R. Napiwotzki, and M. K. Harrop-Allin. "Re j0317-853: The most massive known isolated white dwarf." *Monthly Notices of the Royal Astronomical Society* 277, no. 3 (1995): 971–985. https://doi.org/10.1093/mnras/277.3.971

[46] Leung, S.-C., M.-C. Chu, L.-M. Lin, and K.-W. Wong. "Dark-matter admixed white dwarfs." *Physical Review D* 87, no. 12 (2013): 123506.

[47] Sahoo, R., S. Mukhopadhyay, and M. Bhuyan. "Dark matter admixed white dwarfs: A single-fluid approach." *Physical Review D* 113, no. 12 (2026): 123005.

[48] Boshkayev, K., T. K. Konysbayev, E. B. Kurmanov, M. Muccino, and G. Zhumakhanova. "Physical properties of dark matter in galaxy U11454." *Physical Sciences and Technology* 7, no. 3-4 (2020): 11–20. https://phst.kaznu.kz/index.php/journal/article/view/216

[49] Nunes, S. P., J. D. V. Arbañil, J. M. Z. Pretel, and S. B. Duarte. "Dark matter in White Dwarfs: Implications for their structure." *Journal of High Energy Astrophysics* 50 (2026): 100505.

[50] Kurmanov, Y., K. Boshkayev, T. Konysbayev, M. Muccino, A. Urazalina, G. Ikhsan, N. Saiyp, G. Rabigulova, M. Karlinova, G. Suliyeva, A. Taukenova, and N. Beissen. "Analysis of dark matter profiles in the halos of spiral galaxies." *Physical Sciences and Technology* 10, no. 3-4 (2023): 4–16. https://phst.kaznu.kz/index.php/journal/article/view/347

[51] Boshkayev, K., T. Konysbayev, E. Kurmanov, O. Luongo, M. Muccino, H. Quevedo, A. Taukenova, A. Urazalina, and G. Zhumakhanova. "Motion of stars near the galactic center." *International Journal of Mathematics and Physics* 12, no. 2 (2021): 79–86. https://ijmph.kaznu.kz/index.php/kaznu/article/view/402

[52] Parmar, V., D. Scordino, and I. Bombaci. "Triggering electron capture supernovae: Dark matter effects in degenerate white-dwarf-like cores of super-asymptotic giant branch stars." *Journal of High Energy Astrophysics* 50 (2026): 100470.

Information about authors

Viren Ollivier *– Élève ingénieur polytechnicien (Engineer Student), École Polytechnique, Palaiseau, France, e-mail: viren.ollivier@polytechnique.org*
Md Saifullah Mansur *– BSc Student at the Department of Theoretical and Nuclear Physics, Al-Farabi Kazakh National University, Almaty, Kazakhstan, e-mail: saifullahmansur472@gmail.com*
Nurzada Beissen *– Professor at the Department of Theoretical and Nuclear Physics, Al-Farabi Kazakh National University, Almaty, Kazakhstan, e-mail: nurzada.beissen@gmail.com*
Aigerim Abylayeva *– PhD Student at the Department of Theoretical and Nuclear Physics, Al-Farabi Kazakh National University, Almaty, Kazakhstan, e-mail: abylayeva.aigerim@gmail.com*